Spin, charge, and orbital order in Mn2OBO3

Spin, charge, and orbital order in Mn_2OBO_3

Richard J. Goff,[1,2] Anthony J. Williams,[1] and J. Paul Attfield[1]
[1]*Centre for Science at Extreme Conditions, University of Edinburgh, Erskine Williamson Building, King's Buildings, Mayfield Road, Edinburgh EH9 3JZ, United Kingdom*
and School of Chemistry, University of Edinburgh, Joseph Black Building, King's Buildings, West Mains Road, Edinburgh EH9 3JJ, United Kingdom
[2]*Department of Chemistry, University of Cambridge, Lensfield Road, Cambridge CB2 1EW, United Kingdom*
(Received 10 March 2004; revised manuscript received 5 May 2004; published 23 July 2004)

The magnetic ordering in Mn_2OBO_3 has been determined from neutron diffraction and magnetization measurements. Long range antiferromagnetic order occurs below $T_N=26$ K, other apparent magnetic transitions are due to secondary phases. The magnetic order has a $(\frac{1}{2}0\frac{1}{2})$ propagation vector and the antiferromagnetic spin arrangement has been refined. The low ordering temperature and ordered moment ($1.0\ \mu_B$) at the Mn^{3+} sites evidence magnetic frustration arising from the charge and orbital ordered arrangement of Mn^{2+} and Jahn-Teller Mn^{3+} states. This is supported by a qualitative assessment of the Mn-O-Mn superexchange interactions.

DOI: 10.1103/PhysRevB.70.014426 PACS number(s): 75.25.+z, 61.12.Ld, 75.50.Ee, 71.70.Ch

I. INTRODUCTION

The interplay of spin, charge and orbital degrees of freedom in solid transition metal compounds is of current interest. Semivalent materials are particularly useful as they display the simplest (1:1) charge ordered ground states which, when lattice disorder is minimal, are often sufficiently long range ordered to be observed in crystallographic studies. Any orbital order that breaks the degeneracy of localized-ion states can also be found from structure refinement, and neutron diffraction permits the spin order resulting from the superexchange between the localized moments to be determined. Examples of well-ordered, semivalent transition metal oxides that show long range spin, charge and orbital order are the perovskite types $La_{0.5}Ca_{0.5}MnO_3$,[1] $YBaMn_2O_5$,[2] $YBaCo_2O_5$,[3] $TbBaFe_2O_5$,[4] and $TbBaMn_2O_6$,[5] and the spinel magnetite (Fe_3O_4).[6,7] Semivalent behavior can also be found in more complex networks such as the homometallic warwickite structure.

Many mixed metal oxyborates $MM'OBO_3$ adopt the warwickite structure,[8] where M and M′ are, respectively, a divalent and a trivalent metal. Homometallic (M=M′) warwickites are known only for M=Fe (Refs. 9–11) or Mn.[12,13] The aristotype orthorhombic warwickite structure is based on hexagonal close packing of oxygen ions. The metal ions have octahedral coordination, these octahedra share edges to form ribbons of four infinite chains of octahedra linked by corner sharing and the trigonal planar BO_3 groups. The warwickite structure has two inequivalent sites for the metal ions (M(1) and M(2)), as can be seen in Fig. 1. The homometallic warwickites have been of previous interest because the iron and manganese compounds show different types of charge ordering. Mn_2OBO_3 has the divalent and trivalent ions on different crystallographic sites,[12] i.e., $Mn(1)^{3+}Mn(2)^{2+}OBO_3$ but Fe_2OBO_3 has equal numbers of divalent and trivalent ions on each site, i.e., $Fe(1)^{2+}_{0.5}Fe(1)^{3+}_{0.5}Fe(2)^{2+}_{0.5}Fe(2)^{3+}_{0.5}OBO_3$.[9–11] The different charge orderings within these materials lead to different monoclinic distortions of the orthorhombic warwickite structure.

Fe_2OBO_3 undergoes a charge ordering transition at 317 K, at which the orthorhombic *Pmcn* to monoclinic $P2_1/c$ structural distortion is observed. Magnetic order occurs below $T_C=155$ K. The magnetic structure of Fe_2OBO_3 is L-type ferrimagnetic.[9–11] Magnetic moments on the Fe(1) and Fe(2) chains are antiparallel, so the magnetic structure is almost antiferromagnetic, but the symmetry inequivalence of the two sites leads to an inexact cancellation and a small ferrimagnetic moment of $\sim 0.06\ \mu_B$ per formula unit results.

Mn_2OBO_3 was first prepared by Norrestam *et al.*[12] by annealing $Mn(NO_3)_2.4H_2O$ and H_3BO_3 at 700°C for 3 days, and crystals were grown from a borax flux. The 300 K

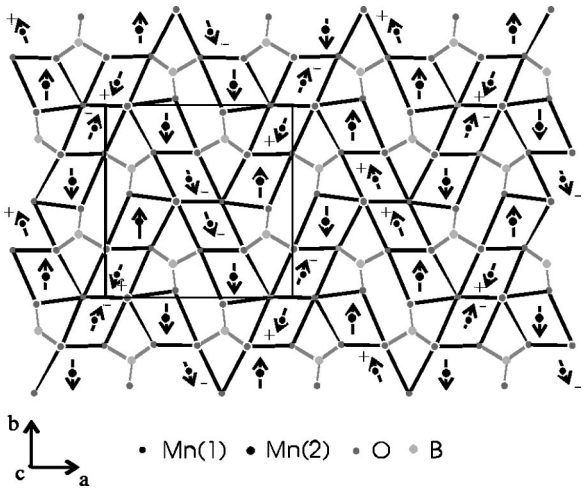

FIG. 1. The crystal and magnetic structures of Mn_2OBO_3 projected on the *ab* plane showing the relative moment direction for Mn atoms at $z=1/4$ and $z=3/4$. The unit cell of the crystal lattice is shown.

structure was found to crystallize in the $P112_1/n$ monoclinic subgroup of *Pmcn*. Full Mn^{2+}/Mn^{3+} charge ordering was revealed by the difference in bond valence sums at the two sites. Orbital order was revealed by a pronounced axial elongation of the $Mn(1)O_6$ octahedra, this is a typical Jahn-Teller distortion for Mn^{3+}. Specific heat and magnetization studies on Mn_2OBO_3 were subsequently carried out,[13] a magnetic transition at 104 K to an antiferromagnetic state with weak ferromagnetism below 70 K was reported. In this paper we report the low temperature spin ordering in Mn_2OBO_3 based on a powder neutron diffraction and magnetization study.

II. EXPERIMENT

An 8 g sample of polycrystalline Mn_2OBO_3 was prepared by heating MnO and H_3BO_3 in air at 800 °C for three days, and then reheating for three periods of three days under argon at 800 °C. The sample was reground between these periods of heating. The powder x-ray diffraction pattern of the sample agreed with that obtained by Norrestam *et al.*;[12] Rietveld analysis showed that the sample also contained 1 wt % of Mn_3O_4. This impurity could not be eliminated by varying the preparation conditions, samples heated for longer times also contained Mn_2O_3. Magnetizations were measured on a superconducting quantum interference device magnetometer. Data were recorded in a 500 Oe field while warming the sample from 5 to 300 K in 1 K steps, following zero field cooling (ZFC), and field cooling (FC).

Neutron diffraction patterns were obtained in the range 10 to 60 K in 10 K intervals on OSIRIS, ISIS facility, Rutherford Appleton Laboratory, UK. OSIRIS is optimized for measurements at long *d*-spacings with a high resolution and a high counting rate;[14] six out of the eight possible detector modules were deployed in these measurements. The high flux of neutrons on OSIRIS allowed the sample of Mn_2OBO_3 containing natural B to be used. The sample of around 8 g was held in a flat plate aluminum can to minimize the effect of neutron absorption by boron-10. Data were collected in the range $d=1.4$ to 6.3 Å. The 10 K data were collected for 12 h, other patterns were recorded in 6 h.

III. RESULTS

A. Crystal structure

Powder neutron diffraction patterns of Mn_2OBO_3 for $d=3.5-5.5$ Å are shown in Fig. 2. The crystal structure was fitted to the 60 K data, with the $P2_1/n$ symmetry structure determined by Norrestam *et al.*[12] as a starting model. The GSAS software package[15] was used to carry out all structural and magnetic refinements. The refined 60 K lattice parameters in the *b*-unique monoclinic setting were $a=9.2919(7)$ Å, $b=9.5311(7)$ Å, $c=3.2438(3)$ Å and $\beta=90.733(2)°$. The atomic coordinates obtained were in agreement with those obtained by Norrestam *et al.* but with large experimental uncertainties. These result from poor intensity statistics due to neutron absorption by boron and the presence of several diffraction peaks from a secondary phase of Mn_3O_4. The peaks due to the Mn_3O_4 and the aluminum sample can were excluded from the refinement.

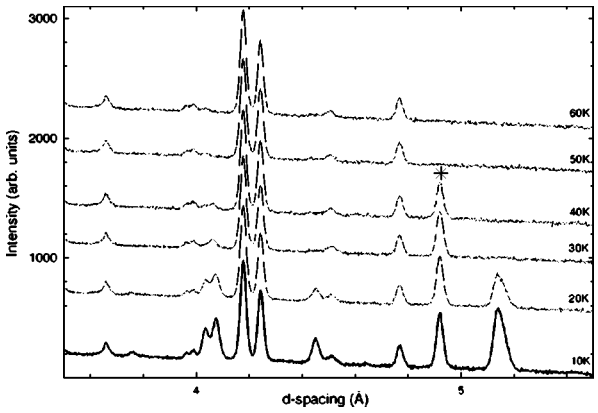

FIG. 2. Neutron diffraction profiles of the Mn_2OBO_3 sample from 10 to 60 K. The Mn_3O_4 (101) magnetic peak is marked with an asterisk.

B. Magnetic structure

Figure 2 shows that on cooling, a prominent magnetic diffraction peak (marked with an asterisk) appears at $d=4.9$ Å in the 40 K profile. This magnetic Bragg peak is not indexed on the Mn_2OBO_3 cell but can be indexed as the Mn_3O_4 (101) reflection. This peak is more intense than might be expected from 1% of an impurity because of microabsorption—the minority phase does not contain boron whereas the principal phase does. A further set of magnetic Bragg peaks appears between 30 and 20 K—these arise from the magnetic ordering in the principal Mn_2OBO_3 phase. The magnetic structure of Mn_2OBO_3 was determined from a (10 K−30 K) difference profile (Fig. 3), obtained by subtracting the 30 K neutron scattering from the 10 K pattern with appropriate scaling to allow for the different counting times. This removes the Mn_2OBO_3 nuclear scattering and the nuclear and magnetic scattering from Mn_3O_4 from the 10 K data, leaving only the Mn_2OBO_3 magnetic scattering.

The magnetic Bragg peaks of Mn_2OBO_3 were all indexed by the $(\frac{1}{2}0\frac{1}{2})$ propagation vector. To fit the magnetic structure, a magnetic supercell (*m* subscripts) related to the structural cell by the following transformation was used,

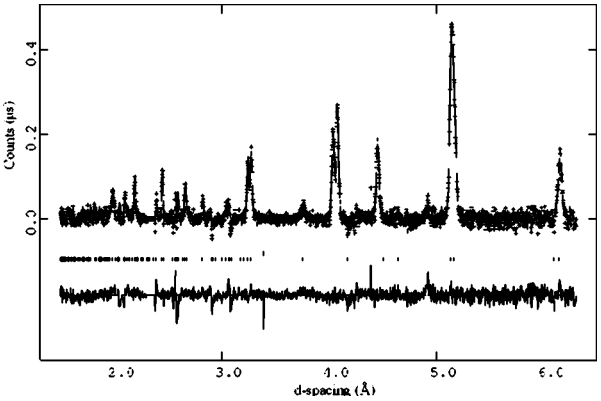

FIG. 3. Observed, calculated and difference Rietveld plots for the magnetic structure fit to the (10 K−30 K) neutron scattering difference profile of Mn_2OBO_3.

TABLE I. The positions and refined magnetic moment components (μ_x, μ_y, and μ_z are parallel to $\mathbf{a}_m$, $\mathbf{b}_m$ and $\mathbf{a}_m$x$\mathbf{b}_m$ respectively) of the unique Mn sites in the $P2_1/c$ magnetic supercell. The Shubnikov (magnetic) group symmetry is also $P2_1/c$.

Site	x	y	z	$\mu_x(\mu_B)$	$\mu_y(\mu_B)$	$\mu_z(\mu_B)$
Mn(1)	−0.3860	0.3836	0.1713	−0.41(9)	−0.84(3)	−0.19(7)
Mn(1)′	−0.8860	0.3836	0.6713	0.41(9)	0.84(3)	0.19(7)
Mn(2)	−0.1953	0.4028	−0.0252	0	4.40(7)	0
Mn(2)′	−0.6953	0.4028	−0.5252	0	−4.40(7)	0

$$\begin{pmatrix} a_m \\ b_m \\ c_m \end{pmatrix} = \begin{pmatrix} -1 & 0 & 1 \\ 0 & 1 & 0 \\ 1 & 0 & 1 \end{pmatrix} \begin{pmatrix} a \\ b \\ c \end{pmatrix}.$$

This cell has twice the volume of the structural cell and has $P2_1/c$ space group symmetry. The magnetic basis consists of two spins at (x,y,z) and $\left(x+\frac{1}{2},y,z+\frac{1}{2}\right)$ for each of the independent Mn(1) and Mn(2) sites (Table I) and their equivalent sites under the $P2_1/c$ symmetry group operations. Good fits to the data were obtained only with a time reversal (spin inversion) operation between (x,y,z) and $\left(x+\frac{1}{2},y,z+\frac{1}{2}\right)$ site spins, but with no time reversal operations accompanying the $P2_1/c$ group operations, so the Shubnikov (magnetic symmetry) group is also $P2_1/c$. The Mn(1) moments were found have significant components in the a_mc_m plane and parallel to $\mathbf{b}_m$, but the Mn(2) moments are parallel to $\mathbf{b}_m$. The resultant Mn(1) (Mn^{3+}) and Mn(2) (Mn^{2+}) moments are 0.95(6) and 4.40(7) μ_B respectively. The fit of this antiferromagnetic structure to the (10 K−30 K) difference gave R_p=3.40%, wR_p=3.77% and χ^2=3.35 and the observed, calculated and difference plots are shown in Fig. 3. Views of the spin arrangement are shown in Figs. 1 and 4.

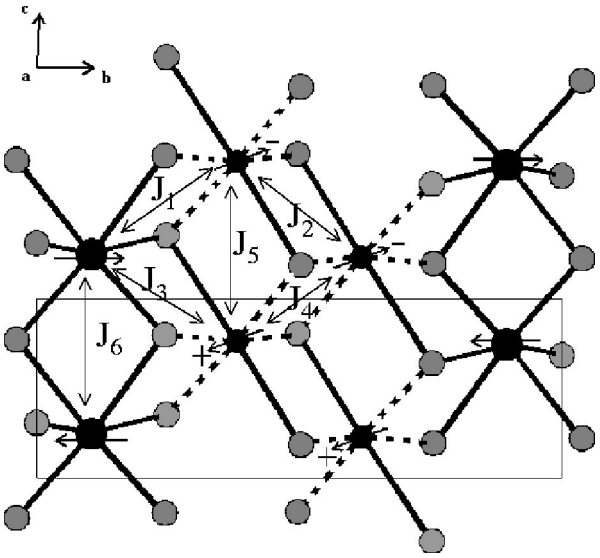

FIG. 4. Magnetic order within the ribbons of four MnO_6 octahedral chains viewed in the *bc* plane. The ordered $d_{x^2-y^2}$ type orbitals containing the e_g holes on Mn^{3+} are shown as broken lines, and the inequivalent superexchange interactions J_1 to J_6 are labeled.

C. Magnetization

The low temperature ZFC and FC magnetic susceptibilities of the Mn_2OBO_3 sample are shown in Fig. 5. Only two magnetic transitions are evident and these are assigned by comparison with the evolution of the neutron scattering in Fig. 2. Mn_3O_4 has a ferrimagnetic ordering transition at 42 K,[16] which dominates the FC magnetization. The second transition, observed at 26 K through the change in slope of the ZFC data, is coincident with the onset of antiferromagnetic ordering seen in the neutron patterns of Mn_2OBO_3. Hence, Mn_2OBO_3 has only one intrinsic magnetic transition down to 4 K, a three-dimensional antiferromagnetic ordering at T_N=26 K.

IV. DISCUSSION

The variable temperature neutron diffraction experiments reveal the intrinsic magnetic ordering in Mn_2OBO_3. A previous study[13] reported an antiferromagnetic transition at 104 K and weak ferromagnetism below 70 K for this phase, and our magnetization data taken alone would suggest a ferromagnetic or ferrimagnetic ordering at 42 K. However, neutron diffraction demonstrates that only a Neel transition to a three-dimensional spin ordering at 26 K is intrinsic to Mn_2OBO_3, and all the other transitions are due to impurity phases such as Mn_3O_4 which has T_C=42 K. This reflects the difficulty in preparing phase-pure samples of complex oxyborates.

The previously reported structure shows that Mn_2OBO_3 is a charge and orbitally ordered insulator at 300 K, and no changes are found down to 10 K in our study. The spin or-

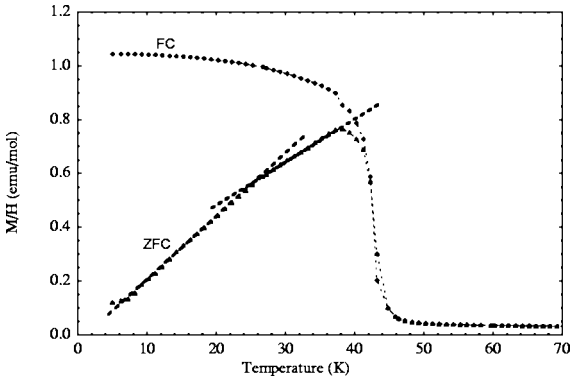

FIG. 5. Magnetization/field measurements of the Mn_2OBO_3 sample in ZFC and FC conditions.

dering at 26 K is dictated by the structural and orbital topology of the structure, as shown in Figs. 1 and 4. The structure results in considerable frustration of the magnetic exchange interactions. The order within the chains of edge-sharing octahedra (repeat period **b**) is antiferromagnetic, so exchange interactions with neighbouring chains are frustrated by the **b**/2 offset between neighboring chains within the ribbons of four chains (Fig. 1). Triangular connections through the BO_3 groups (Fig. 1) create further magnetic frustration. Reduction in the ordered moment commonly results from topological frustration. A striking feature of the magnetic structure of Mn_2OBO_3 is that the Mn(2) moment of 4.4 μ_B is as expected for $S=\frac{5}{2}$ Mn^{2+}, allowing for typical covalent and zero-point reductions from the ideal value of 5 μ_B, but the Mn(1) site moment of 1.0 μ_B is greatly reduced from the ideal value of 4 μ_B for $S=2$ Mn^{3+}.

To gain insight into the ordered spin arrangement and the moment reduction of the Mn^{3+} sites in Mn_2OBO_3, estimates of the superexchange interactions are needed. Many inequivalent superexchange pathways are present in this complex network, but the dominant interactions are mediated through the MnO_2Mn bridges between edge-sharing MnO_6 octahedra, as shown in Fig. 4. The ferro- or antiferromagnetic nature of each Mn-O-Mn connection depends primarily on the e_g electron density in the Mn-O bonds, i.e., upon the orbital ordering. For charge ordered Mn^{3+}/Mn^{4+} arrangements such as $(La_{0.5}Ca_{0.5})MnO_3$,[1,17] the sign of the superexchange interactions predicted from the orbital ordering is consistent with the complex CE-type magnetic arrangement. Orbitally non-degenerate Mn^{4+} states (d^3) have no e_g electrons, whereas Mn^{3+} states (d^4) have one e_g electron, so the presence of one e_g electron per $Mn^{3+}+Mn^{4+}$ pair is key; the density of this electron is associated with the Mn^{3+} d_z^2 orbital identified with a pair of elongated Mn-O bonds. In a charge ordered Mn^{2+}/Mn^{3+} arrangement as found in Mn_2OBO_3, orbitally non-degenerate Mn^{2+} has both e_g orbitals singly occupied, whereas Mn^{3+} states have only one e_g electron, so each $Mn^{2+}+Mn^{3+}$ pair has one e_g hole. This e_g hole density is in the Mn^{3+} $d_{x^2-y^2}$ type orbital associated with four short, coplanar Mn-O bonds.

The orbital ordering of the e_g holes within the ribbons of four octahedral chains is shown in Fig. 4, together with the six distinct MnO_2Mn superexchange bridges J_1 to J_6. The ferromagnetic (F) or antiferromagnetic (AF) natures of the two Mn-O-Mn contributions to each bridge are listed in Table II. The Mn-O-Mn angles are distorted from 90 (with values from 75° to 91°) so it is assumed, following the Goodenough-Kanomouri rules[18] that $e_g^1-O:2p-e_g^1$ contributions (to J_3 and J_6) are AF, whereas $e_g^1-O:2p-e_g^0$ overlaps (in J_1, J_2, J_3, J_5) are F. In the case of $e_g^0-O:2p-e_g^0$ orbital combinations (J_4), $t_{2g}^1-O:2p-t_{2g}^1$ overlap will lead to weaker π-type AF interactions. This simple approach gives an unambiguous prediction of the sign for all of the interactions except J_3. The observed spin alignments (Table II) agree with four of the five predicted interactions (J_1, J_2, J_4, J_6), but the remaining J_5 interaction is frustrated. J_5 favors a ferromagnetic alignment of moments within the Mn(1) chains (Fig. 4) but this is evidently outweighed by the J_2+J_4 and J_1+J_3 interactions through neighboring chains that lead to an antiparallel alignment of spins in the Mn(1) chains. This frustration of the intrachain exchange by the interchain interactions provides an explanation for why the ordered moments in the Mn(1) (Mn^{3+}) chains are considerably reduced by frustration, whereas the Mn(2) (Mn^{2+}) site moments are unaffected.

TABLE II. Predicted superexchange interactions and the observed angle between moment directions for the six MnO_2Mn bridges in Fig. 4. For each bridge, the predicted contribution of the two Mn-O-Mn linkages is shown as ferromagnetic (F) or antiferromagnetic (AF). Participating orbitals at the orbitally ordered Mn^{3+} sites are given.

J_i	Mn-(-O-)-Mn superexchange bridge (expected interaction)	Observed angle between moments
J_1	$Mn^{2+}:e_g^1$-$Mn^{3+}:(d_{x^2-y^2})^0$(F) $Mn^{2+}:e_g^1$-$Mn^{3+}:(d_{x^2-y^2})^0$(F)	27.8°
J_2	$Mn^{3+}:(d_z^2)^1$-$Mn^{3+}:(d_{x^2-y^2})^0$(F), $Mn^{3+}:(d_{x^2-y^2})^0$-$Mn^{3+}:(d_z^2)^1$(F)	0°
J_3	$Mn^{2+}:e_g^1$-$Mn^{3+}:(d_z^2)^1$(AF), $Mn^{2+}:e_g^1$-$Mn^{3+}:(d_{x^2-y^2})^0$(F)	152.2°
J_4	$Mn^{3+}:(d_{xz})^1$-$Mn^{3+}:(d_{yz})^1$(AF), $Mn^{3+}:(d_{yz})^1$-$Mn^{3+}:(d_{xz})^1$(AF)	180°
J_5	$Mn^{3+}:(d_z^2)^1$-$Mn^{3+}:(d_{x^2-y^2})^0$(F), $Mn^{3+}:(d_{x^2-y^2})^0$-$Mn^{3+}:(d_z^2)^1$(F)	180°
J_6	$Mn^{2+}:e_g^1$-$Mn^{2+}:e_g^1$(AF) $Mn^{2+}:e_g^1$-$Mn^{2+}:e_g^1$(AF)	180°

Frustration of the magnetic interactions that result from the charge and orbital ordering also accounts for the difference in spin ordering between Mn_2OBO_3 and Fe_2OBO_3. Fe_2OBO_3 is an L-type ferrimagnet with a Curie temperature of 155 K, whereas the Neel temperature of Mn_2OBO_3 is only 26 K. In Fe_2OBO_3, which is not orbitally ordered, the spin chains are ferromagnetic and the antiferromagnetic interchain interactions are satisfied so the magnetic arrangement is relatively unfrustrated. Mn_2OBO_3 has a strong orbital ordering in the Mn(1) chains occupied by Mn^{3+}. The orbital ordering results in a complex pattern of ferro- and antiferro-magnetic superexchange interactions that frustrates long range magnetic order, so that spin ordering takes place only at the relatively low temperature of 26 K.

ACKNOWLEDGMENTS

The authors thank the EPSRC for the provision of neutron beamtime at ISIS and studentships for R.J.G. and A.J.W., and Dr. Ken Anderson for providing assistance with the neutron measurements.

[1] P. G. Radaelli, D. E. Cox, M. Marezio, and S-W. Cheong, Phys. Rev. B **55**, 3015 (1997).
[2] F. Millange, E. Suard, V. Caignaert, and B. Raveau, Mater. Res. Bull. **34**, 1 (1999).
[3] T. Vogt, P. M. Woodward, P. Karen, B. A. Hunter, P. Henning, and A. R. Moodenbaugh, Phys. Rev. Lett. **84**, 2969 (2000).
[4] P. Karen, P. M. Woodward, J. Linden, T. Vogt, A. Studer, and P. Fischer, Phys. Rev. B **64**, 214405 (2001).
[5] A. J. Williams and J. P. Attfield, Phys. Rev. B **66**, 220405(R) (2002).
[6] J. P. Wright, J. P. Attfield, and P. G. Radaelli, Phys. Rev. Lett. **87**, 266401 (2001).
[7] J. P. Wright, J. P. Attfield, and P. G. Radaelli, Phys. Rev. B **66**, 214422 (2002).
[8] Y. Takeuchi, T. Watanabe, and T. Ito, Acta Crystallogr. **3**, 98 (1950).
[9] J. P. Attfield, A. M. T. Bell, L. M. Rodriguez-Martinez, J. M. Greeneche, R. Retoux, M. Leblanc, R. J. Cernik, J. F. Clarke, and D. A. Perkins, J. Mater. Chem. **9**, 205 (1999).
[10] J. P. Attfield, A. M. T. Bell, L. M. Rodriguez-Martinez, J. M. Greeneche, R. J. Cernik, J. F. Clarke, and D. A. Perkins, Nature (London) **396**, 655 (1998).
[11] J. P. Attfield, J. F. Clarke, and D. A. Perkins, Physica B **180**, 581 (1992).
[12] R. Norrestam, M. Kritikos, and A. Sjodin, J. Solid State Chem. **114**, 311 (1995).
[13] M. A. Continentino, A. M. Pedreira, R. B. Guimaraes, M. Mir, J. C. Fernandes, R. S. Freitas, and L. Ghivelder, Phys. Rev. B **64**, 014406 (2001).
[14] K. H. Andersen, D. M. Y. Marero, and M. J. Barlow, Appl. Phys. A: Mater. Sci. Process. **74**, S237 (2002).
[15] A. C. Larson and R. B. Von Dreele, Los Alamos National Laboratory Report No. LAUR 86-748 (1994).
[16] K. Dwight and N. Menyuk, Phys. Rev. **119**, 1470 (1960).
[17] J. B. Goodenough, Phys. Rev. **100**, 564 (1955).
[18] J. B. Goodenough, *Magnetism and the Chemical Bond* (Interscience, New York, 1963).